

Composite Tissue-Type and Probability Image for Ultrasound and Microwave Tomography

Pedram Mojabi, *Graduate Student Member, IEEE*, and Joe LoVetri, *Senior Member, IEEE*

Abstract—The concept of creating a composite tissue-type-image (cTTI) along with an associated probability image is introduced for ultrasound and microwave tomography. The cTTI integrates information available within different quantitative property images, and the associated probability image provides an indication of the level of confidence regarding the reconstructed tissue types. It is shown that the cTTI concept can be applied to ultrasound tomography property images, microwave tomography property images, as well as to their combination. Thus, the concept is generalizable to the amalgamation of quantitative information derived from a wide variety of modalities with the goal of increasing the confidence in the reconstructed cTTI. Validation of the concept is performed on MRI-derived numerical breast phantoms containing up to five different tissue types.

Index Terms—Breast imaging, inverse scattering, microwave tomography (MWT), probability density function (PDF), tissue-type image (TTI), ultrasound tomography (UT).

I. INTRODUCTION

ULTRASOUND tomography (UT) and microwave tomography (MWT) are two quantitative imaging modalities which are being investigated for several industrial nondestructive testing and biomedical imaging applications [1]–[8]. The focus of this study is on the application of these techniques to biomedical breast tissue imaging. Both of these imaging modalities rely on irradiating the object of interest (OI) using incident waves (pressure waves in UT, and electromagnetic waves in MWT). The scattered waves from the OI are collected and then utilized to reconstruct images of related properties of the OI. In UT, these properties are the ultrasonic properties, for example, in this study, we consider the compressibility, attenuation, and density profiles. In MWT, the properties of interest are the real and imaginary parts of the complex permittivity profile of the OI.

Both of these modalities can be mathematically formulated as an inverse scattering problem, which is nonlinear and ill-posed. Several nonlinear inversion algorithms have been utilized in the past to solve these problems, for example, the Born iterative method (BIM) [9]–[12], the distorted BIM [13]–[16], and the contrast source inversion algorithm [17], [18]. Generally, such methods need to be applied in conjunction with regularization techniques, such as the standard Tikhonov [19], [20], the L_1 -

Manuscript received November 11, 2015; revised February 9, 2016 and April 6, 2016; accepted April 26, 2016. Date of publication April 28, 2016; date of current version June 6, 2016.

The authors are with the Department of Electrical and Computer Engineering, University of Manitoba, Winnipeg, MB R3T 2N2, Canada (e-mail: Pedram.Mojabi@UManitoba.ca; Joe.LoVetri@UManitoba.ca).

Color versions of one or more of the figures in this paper are available online at <http://ieeexplore.ieee.org>.

Digital Object Identifier 10.1109/JMMCT.2016.2560625

norm Tikhonov [21], [22], multiplicative regularizers [23], [24], truncated singular value decomposition [25], [26], and conjugate gradient least squares (CGLS) subspace regularization methods [4], [5], [10], [25]. These regularization techniques are used to deal with the ill-posedness of the inverse problem.

We have recently shown how to reconstruct the three aforementioned ultrasonic properties of the OI using the BIM inversion algorithm in conjunction with the CGLS regularization technique [10]. We have also shown how to improve the reconstruction of the contrast profiles using a balancing method for the case that the ranges of the contrast profiles are significantly different from each other [27]. Similarly, several inversion algorithms have been proposed to reconstruct the complex permittivity profile of the OI using MWT data [4], [5]. Thus, UT and MWT inversion algorithms exist to solve the inverse scattering problem and thereby produce quantitative images corresponding to the relevant physical properties associated with the respective wave propagation.

Often, especially in biomedical imaging, the goal is to infer the tissue type within the image, but this can be quite difficult working from a single-property image such as ultrasonic wave speed. Even when three ultrasonic properties are reconstructed simultaneously, as in [10], it is difficult to infer the tissue-type at a particular pixel location. Techniques to do so are typically *ad hoc*, relying on the expertise of the person examining the image. Recently, we have proposed preliminary systematic techniques to create such tissue-type images (TTIs) [28], [29]. In this paper we introduce a general systematic procedure, based on Bayesian inference, to derive a TTI from one or more property images.

Thus, three quantitative property images obtained from UT data, and/or two quantitative property images obtained from MWT, are utilized to form a single TTI which we refer to as the composite tissue-type image (cTTI). Each tissue type in the inferred cTTI is represented by a single color. This approach offers the following advantages. First, the cTTI is more robust and reliable than a TTI derived from a single quantitative image because the most accurately reconstructed part of each property image is used toward the creation of the cTTI. Second, for each pixel of the cTTI, we construct an associated probability value that indicates the level of confidence regarding the assignment of the final tissue type to that pixel. (It should be emphasized that current UT and MWT algorithms do not provide any indications regarding the level of confidence in their reconstruction, which is a serious disadvantage for risk assessment associated with a diagnosis.) Third, a physician can more easily understand the cTTI without knowing the ultrasonic or complex permittivity values of different tissues. The cTTI, along with the associated probability image, can provide the physician with better

information that is required to evaluate patient health and risk factors. In addition, the physician would be provided with a single image as opposed to several images obtained from different imaging modalities.

For the creation of this cTTI, we require 1) quantitative reconstructions of at least two properties of the OI, and 2) the probability density functions (PDF) for the property values corresponding to the different tissues within the object being imaged. The quantitative property reconstructions can be obtained using any available inversion algorithm. The PDFs of different properties for each tissue are estimated from property-value ranges available in the published literature [5], [30]–[36].

We further show that single-property TTIs, or the cTTI, can be used to improve the quantitative reconstructions of the OI. In this method, we first utilize the quantitative reconstructions of the properties to create the TTIs, or the cTTI, and then utilize these to provide a good initial guess for the inversion algorithm (for any of the property reconstructions). As is well known, the appropriate choice of an initial guess is very important for avoiding local minima and converging to a good solution.

The TTI concept presented in this paper can be applied to different biomedical or industrial applications. However, in this paper, we limit ourselves to the breast imaging application. In addition, although we consider 2-D MWT and UT, the framework presented in this paper can be applied to 3-D problems as well. The structure of this paper is as follows. In Section II, the problem statement is presented. Then, two methods to create the composite TTI based on using the quantitative reconstruction of the properties of the OI are described in Section III. Results of applying the techniques to MRI derived numerical phantoms are then presented and discussed in Section IV.

II. PROBLEM STATEMENT AND METHODOLOGY

The methodology for creating the TTIs and the cTTI is independent of the number and type of property images that are used. We, thus, describe the methodology as a general procedure, but subsequently apply it to three cases in Section IV. That is, we validate the methodology using quantitative UT images, or quantitative microwave (MW) images, or combinations of these.

A. Tissue Property Data

A basic assumption of creating TTIs is that, not only is there some correlation between tissue properties and tissue types, but that the tissue properties provide a means of discriminating between different tissues of interest. As the discrimination capacity of a single property may not be ideal, the use of several properties reinforces the discrimination. In order to perform such a function quantitatively and in a systematic way, it is assumed that typical property values for specific tissue types are available and that PDFs of the property values for the tissues of interest can be estimated. This basic assumption is required for the methodology that will be presented, and the inferences made about the tissue type at any particular pixel depend on the form of the PDFs that are assumed. Nonetheless, the procedure itself is independent of the form of the PDFs. If future experimental

work reveals more accurate property distributions for some or all of the tissues of interest, the methodology can easily incorporate these. For the examples shown in Section IV, we describe how we approximate Gaussian PDFs for five properties of five different tissue types.

B. MW and Ultrasound (US) Property-Image Formation

The TTIs are inferred from property images, and thus, a means of creating US and MW property images is required. In this study, we focus on three US properties, i.e., compressibility, attenuation, and density, as well as two MW properties, i.e., the real and imaginary parts of the complex permittivity. It is assumed that the US and MW inverse scattering problems have been solved resulting in five quantitative images for these properties. For the results considered herein, the US inverse scattering problem is solved using the algorithm presented in [10] and [27], and the MW inverse scattering problem is solved using the algorithm presented in [37]. These are representative of state-of-the-art inversion algorithms available in the literature.

III. FORMATION OF THE COMPOSITE TTI

Two methods to create cTTIs are described and investigated. The first method first forms single-property TTIs along with their corresponding probability images and then uses these to construct a cTTI. In the second method, all the property images of interest are used simultaneously to create the cTTI, bypassing the creation of the single-property TTIs. Along with the reconstructed quantitative images obtained from UT and/or MWT, both require approximate PDFs of property values for each tissue being considered. The first method requires only single-variate PDFs for each combination of property/tissue-type pair, whereas the second method utilizes multivariate PDFs for all the properties for each tissue type. The flowchart showing how these two methods work is depicted in Fig. 1.

The goal of the methodology is to construct a cTTI wherein each pixel is labeled, via a specific color, with the most-probable tissue type. The probability of the label being correct is provided by the corresponding probability image. This probability represents the confidence one should have that the particular pixel corresponds to that tissue type given all of the available information.

A. Method 1: cTTI Derived From Single-Property TTIs

The first step of this method is to first construct a single-property TTI and its corresponding probability image for each quantitative property image. Thus, for example, if we have available three quantitative property images, we will obtain six images. These six images are then used to form one composite TTI with a corresponding composite probability image. For US imaging, the properties being imaged will be, e.g., compressibility, attenuation, and density, whereas for MW imaging, the properties will be the real and imaginary parts of the complex permittivity.

The number of tissue types of interest should also be specified. For example, four or five different tissue types can be chosen

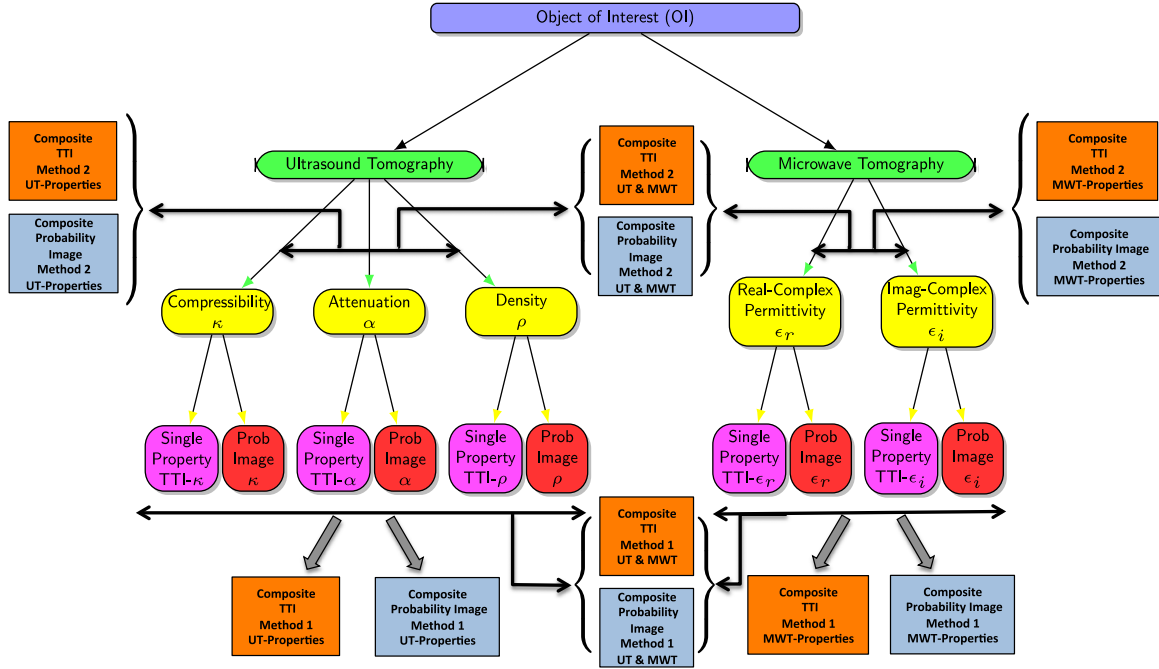


Fig. 1. Flowchart of creating a cTTI using Methods 1 and 2 for both UT and MWT. In Method 1, single-property TTIs and single-property probability images for all the properties of interest are created. This information is then utilized to create the cTTI along with its composite probability image. In Method 2, we do not create single-property TTIs. All the properties of interest are simultaneously utilized to directly create the cTTI along with its composite probability image.

for breast imaging, namely, skin, fat, glandular, tumor, and/or cyst. (The number of chosen tissue types can be adjusted for different applications.)

The steps for creating the single-property tissue-type and probability images are summarized as follows.

- 1) Consider each of the quantitative property images in turn.
- 2) At each pixel within the quantitative property image, we calculate the probability that pixel corresponds to tissue type, T_k , using Bayes' formula [38]

$$P(T_k|x) = \frac{p(x|T_k)P(T_k)}{\sum_{i=1}^{N_t} p(x|T_i)P(T_i)} \quad (1)$$

where x is the property value of that pixel in the property image. In this formula N_t is the total number of tissues, and $p(x|T_k)$ is the value of the PDF at property value x for tissue T_k . The term $P(T_k)$ is the prior probability of assigning tissue type T_k for that pixel. In this study, we assume no prior information and, therefore, set all of the prior probabilities to be equal among the tissues being considered. That is, for the case that we consider five tissue types, we set $P(T_k) = 0.2$. At the end of this step, we will have N_t probabilities assigned to each pixel, one for each tissue type.

- 3) To form the TTI, we assign each pixel the tissue type with the highest probability calculated in step 2. Thus

$$\text{if } P(T_k|x) > P(T_j|x) \implies \text{choose tissue } T_k \quad (2)$$

where $j = 1, \dots, N_t$ and $j \neq k$.

We also keep this highest probability of each pixel and introduce it at the corresponding pixel in the probability image. Thus, we have two images for each property of interest, as shown in Fig. 1. The first image is called the single-property TTI and the second image is called the single-property probability image.

- 4) Once we obtain the single-property TTI and single-property probability image for this property, we go back to Step 1 and repeat these procedures until all the properties are covered.

Now, we can utilize all these single-property TTIs and single-property probability images to create a cTTI. To this end, for each pixel within the cTTI, we scan all the corresponding pixels in single-property TTIs and their single-property probability images. We then choose the tissue type of the highest probability and assign it to that pixel of the cTTI. We also keep this highest probability to form the composite probability image. This procedure continues until all the pixels of the cTTI are covered.

B. Method 2: cTTI Derived From Simultaneous Use of Different Properties

Whereas Method 1 treated the information within the individual quantitative property images as independent, Method 2 makes some assumptions regarding how this information is correlated. That is, Method 2 forms the cTTI by simultaneously considering all the quantitative images, without creating single-property TTIs, and assumes that for each tissue-type we have available a multivariate PDF that takes into account all of the properties. Although having an accurate multivariate PDF may seem demanding, we will show that simple assumptions

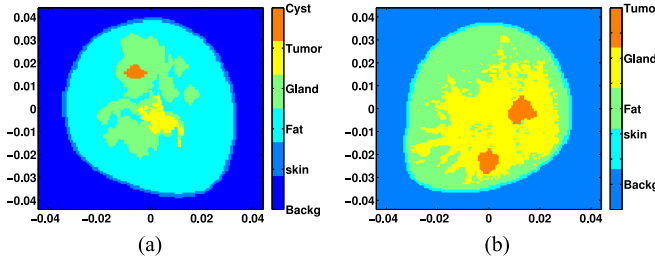


Fig. 2. True TTI for MRI-based numerical breast phantoms. (a) Phantom with a medium sized tumor. (b) Phantom of a dense breast.

as to the form of this multivariate PDF improve the predicted cTTI. Specifically, we assume that a multivariate normal PDF, in d dimensions (corresponding to the number of properties), can be used. Thus, we assume that the multivariate normal PDF for tissue T_k is of the form [38]

$$p(\mathbf{x}|T_k) = \frac{1}{(2\pi)^{d/2} |\Sigma|^{1/2}} \times e^{-\frac{1}{2}(\mathbf{x}-\mu)^t \Sigma^{-1} (\mathbf{x}-\mu)} \quad (3)$$

where \mathbf{x} is a vector of length d corresponding to the value of d properties for each pixel, μ is the mean vector of length d corresponding to the mean value of each property, and Σ is the $d \times d$ covariance matrix. Also, $|\Sigma|$ and Σ^{-1} are the determinant and the inverse of the covariance matrix. For simplicity, it is assumed that the properties are statistically independent; thus, the covariance matrix is diagonal.

The steps of this method are summarized as follows.

- 1) For each pixel, considering all the property images of interest simultaneously, the value of multivariate PDF for each tissue type is calculated based on (3), i.e., $p(\mathbf{x}, T_1), p(\mathbf{x}, T_2), \dots, p(\mathbf{x}, T_k)$.
- 2) The probability that any particular tissue, T_k , occupies a pixel is calculated using Bayes' formula, where (1) is used with vector argument \mathbf{x} rather than x .
- 3) Bayesian decision theory [38] is then applied where the tissue type with the highest probability is assigned to each pixel. As in Method 1, two images will be obtained from this method. The first image is the composite TTI, and the second image is the composite probability image (i.e., the highest probability).

IV. RESULTS

To validate the effectiveness of the TTI methodology, numerical experiments with synthetically derived data were performed. For these experiments, two different 2-D MRI-based numerical phantoms were considered [39]. The first phantom contains a medium-sized tumor and a total of five tissue types: skin, fat, glandular, cyst, and tumor. The second phantom is a dense breast having four tissue types (no cyst) and two medium-sized tumors. The true tissue images of these phantoms are shown in Fig. 2. The discrete colorbar of each image is used to identify the tissue type. Note that for all of the synthetic examples considered herein, noise is added to the scattered field data according to a percentage value of the maximum scattered field. Details are provided in [40].

TABLE I
RANGES OF THE SPEED OF THE SOUND ($c = \frac{1}{\sqrt{\kappa \rho}}$), ATTENUATION AND DENSITY FOR BREAST TISSUES

Tissue	Speed of Propagation [m/s]	Attenuation [$\frac{\text{dB}}{\text{cm MHz}}$]	Density [$\frac{\text{kg}}{\text{m}^3}$]
Skin	$1710 < c < 1750$	$0.65 < \alpha < 0.85$	$1128 < \rho < 1145$
Fat	$1410 < c < 1450$	$0.1 < \alpha < 1$	$941 < \rho < 960.5$
Glandular	$1540 < c < 1570$	$0.8 < \alpha < 1.5$	$963 < \rho < 979$
Tumor	$1575 < c < 1625$	$2.2 < \alpha < 3$	$982 < \rho < 998$
Cyst	$1510 < c < 1540$	$0.1 < \alpha < 0.35$	$1012 < \rho < 1030$

The results are presented in the following format. First, in Section IV-A, the reconstructions of the ultrasonic properties for each phantom are shown. Then, these reconstructions are utilized to create single-property TTIs and cTTIs using Methods 1 and 2. In Section IV-B, the reconstructions of the electromagnetic properties for the phantoms are shown. Then, these quantitative MWT properties are utilized to create single-property TTIs and a cTTI. In Section IV-C, UT and MWT are utilized together to create a cTTI. Finally, in Section IV-D, we show how the concept of cTTI can be used to provide an enhanced initial guess for the inversion algorithm. It should be noted that the prior probabilities for all the tissue types are assumed to be the same unless otherwise stated.

A. cTTI for UT

1) *Formation of the True Quantitative Profile:* The ranges of the ultrasonic properties for breast are shown in Table I. These ranges are chosen based on [30]–[34]. To create numerical phantoms from the MRI-based tissue phantoms for each property being considered, we randomize the property values at each pixel for each tissue. That is, to set the property values for each tissue, we apply a uniformly distributed random function to pick up values for every pixel within that tissue. For example, if the upper and lower ranges of a property associated with a given tissue type is a and b , respectively, the true quantitative values for that property within that tissue are chosen to be $a + (b - a) \times \text{rand}$, where rand is a uniformly distributed random number from 0 to 1.

2) *Formation of the PDFs:* Based on the expected ranges of each property for a given tissue, we create the required PDFs. For example, if we consider five tissue types and five properties, we will have 25 single-variate PDFs. These PDFs are all assumed to have normal distributions with their mean values coinciding with the mean value of the expected range for each property associated with a certain tissue. Furthermore, to find the standard deviation of the PDF, it is assumed that the value of the PDF at the minimum and maximum values of the expected range is 40% of the maximum value of the PDF. These standard deviations and means are also utilized to create the multivariate normal PDF for Method 2.

3) *Inversion Setup:* Three ultrasonic frequencies of operation, $f = [110, 150, 200]$ kHz, are considered. The number of transmitters and receivers is set to be 120 and water is chosen as the background medium. The datasets corresponding to these three frequencies are simultaneously

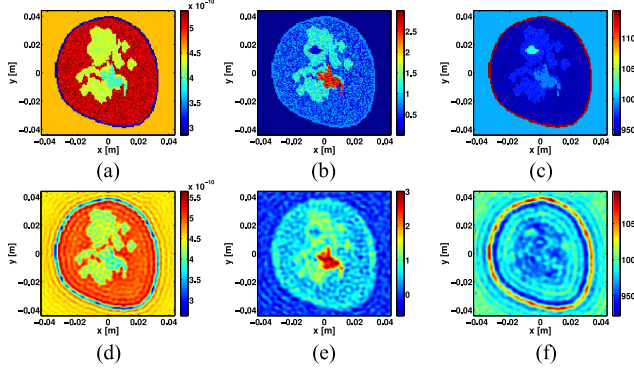


Fig. 3. First row corresponds to the true compressibility, attenuation, and density profiles. The second row corresponds to the reconstruction of compressibility, attenuation, and density profiles for the data contaminated with 2% noise. (a) True κ . (b) True α . (c) True ρ . (d) Reconstructed κ . (e) Reconstructed α . (f) Reconstructed ρ .

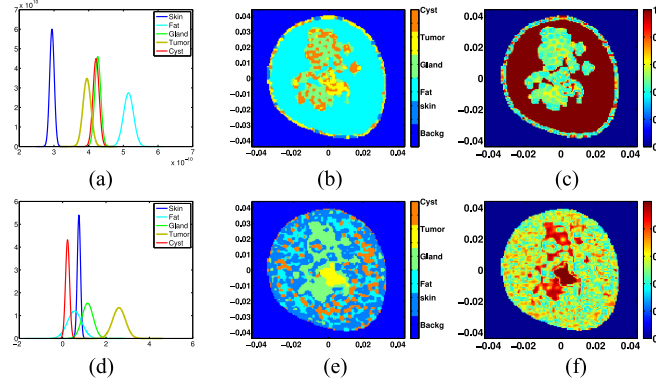


Fig. 4. PDF, single-property TTI, and probability image for compressibility and attenuation are shown in the first and second rows, respectively. (a) PDF κ . (b) Single-property TTI- κ . (c) Probability image κ . (d) PDF α . (e) Single-property TTI- α . (f) Probability image α .

inverted. Due to the fact that attenuation is dependent on frequency, we reconstruct the slope of the attenuation at these frequencies (which can be assumed to be a constant). The term attenuation is used throughout the paper to refer to this quantity.

4) First Phantom (Phantom With a Medium-Sized Tumor): The true TTI for this phantom is shown in Fig. 2(a). The true compressibility, attenuation, and density profiles for this phantom are shown in the top row of Fig. 3. The reconstruction of the properties with 2% noise added to the data is shown in the bottom row of Fig. 3. As can be seen, the reconstruction of the density is poor, and we, thus, do not use this property for creating the composite TTI. That is, we only use reconstructed compressibility and attenuation property images. (It will be shown in Section IV-D that the reconstruction of density can be improved using a good initial guess based on the reconstructed composite TTI.) The PDFs for the compressibility and attenuation for all tissue types are shown in the first column of Fig. 4. Using these PDFs and the reconstructed properties, a single-property TTI and a single-property probability image for each property are constructed. These are shown in the second

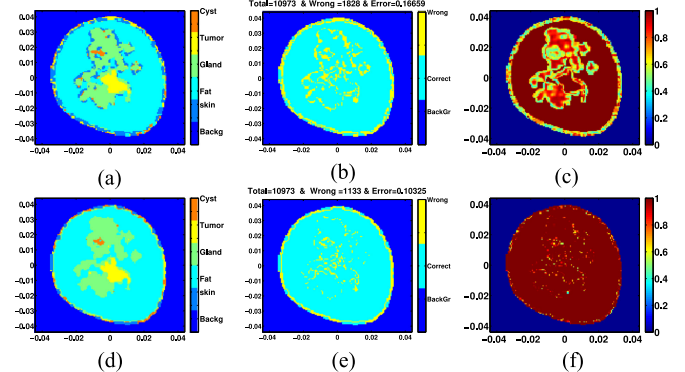


Fig. 5. First and second rows correspond to the reconstruction of a cTTI, correct pixel image, and probability image using Methods 1 and 2, respectively. (a) cTTI-Method 1. (b) Correct pixels. (c) Probability Image. (d) cTTI-Method 2. (e) Correct pixels. (f) Probability image.

and third columns of Fig. 4, respectively. It is worthwhile to note that the fat region can be well distinguished from the other tissues, with high probability values, using the single-property compressibility TTI. The tumor is also well detected using the single-property attenuation TTI, again with high probability values. Note, though, that if one were to utilize only the attenuation property, there would be many false skin designations within the fat region. Similarly, using only compressibility, there would be many false cyst designations within the glandular region.

The cTTI based on κ and α properties can then be created by either Method 1 or Method 2. The cTTI, correct-pixel image, and probability image using Methods 1 and 2 are shown in the first and second rows of Fig. 5, respectively. Here, using two properties, we already see a substantial reduction in the number of false designations of tissue type. As can be seen in the title bar of the correct-pixel images, the error which is defined as the ratio of the number of wrong pixels to the total number of pixels within the OI for the reconstructed cTTI using Method 2 (0.10325) is smaller than that using Method 1 (0.16659).

5) Second Phantom (Dense Breast With Two Tumors): The true TTI for this phantom is shown in Fig. 2(b). The true compressibility, attenuation, and density profiles for this phantom are shown in the first row of Fig. 6. The reconstruction of these properties for two different noise levels (2% and 9%) is shown in the second and third rows of Fig. 6, respectively. The PDF and TTI as well as the probability image for the compressibility and attenuation are shown in the first and second rows of Fig. 7 for the case that the noise level is 2%. Similar to the previous example, it can be seen in Fig. 7 that fat can be well distinguished, with high probability values, from the other tissues using the single-property TTI derived from compressibility. The tumor region can also be well distinguished using the single-property TTI derived from attenuation. The cTTI, correct-pixel image, as well as probability image for both noise levels using Methods 1 and 2 are shown in Fig. 8. As can be seen, this TTI obtained from the 9% noise still allows one to distinguish the tissue types.

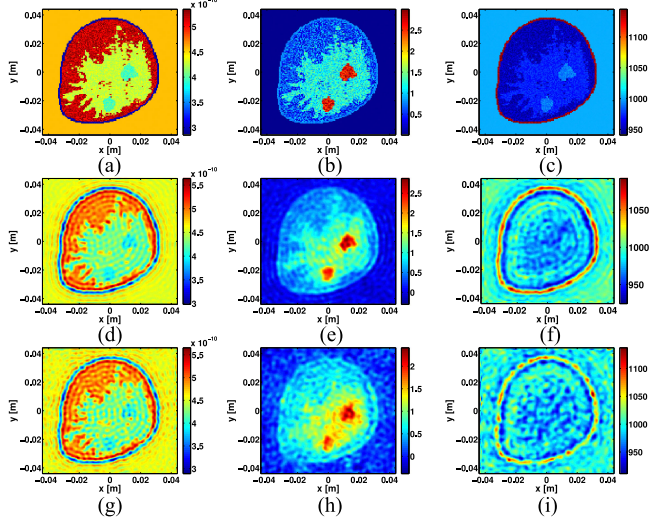


Fig. 6. First row corresponds to the true compressibility, attenuation, and density profiles for dense breast. The second and third rows correspond to the reconstruction of the profiles for 2% and 9% noise, respectively. (a) True κ . (b) True α . (c) True ρ . (d) Reconstructed κ . (e) Reconstructed α . (f) Reconstructed ρ . (g) Reconstructed κ . (h) Reconstructed α . (i) Reconstructed ρ .

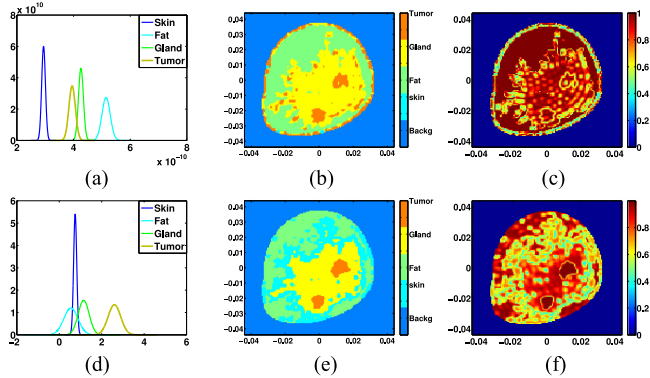


Fig. 7. PDF, single-property TTI, and probability image for the κ and α are shown in the first and second rows for 2% noise. (a) PDF κ . (b) Single-property TTI- κ . (c) Probability image κ . (d) PDF α . (e) Single-property TTI- α . (f) Probability image α .

B. cTTI for MWT

1) *Formation of the True Quantitative Profile and PDFs:* The range of electromagnetic properties for breast at a frequency of 1.1 GHz are shown in Table II. These values are chosen based on values published in [5], [35], and [36]. For each value in this table, we consider $\pm 10\%$ variation. The complex permittivity of the background is assumed to be $23.3 - j18.46$, as in [5]. To create the true quantitative values for each tissue within this phantom, we utilize the same method used for UT explained in Section IV-A1. The formation of PDFs is also the same as the method for UT explained in Section IV-A2.

2) *Inversion Setup:* Five frequencies of operation, $f = [1.1, 1.5, 2, 2.4, 2.8]$ GHz are considered. The datasets corresponding to these frequencies are simultaneously utilized for the inversion. The number of transmitters and receivers is set to be 30. We note that the inversion algorithm takes into account

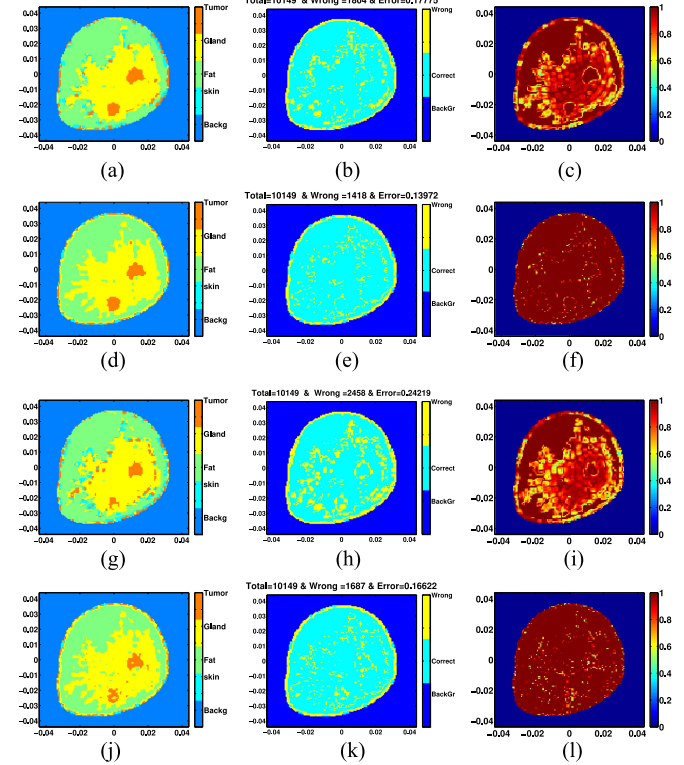


Fig. 8. Create a cTTI based on the reconstruction of κ and α . The first and second rows correspond to the reconstruction of a cTTI, correct pixel image, and probability image based on Methods 1 and 2 for the 2% noise. The third and fourth rows correspond to the cTTI, correct pixel image, and probability image based on Methods 1 and 2 for a 9% noise level. (a) cTTI-Method1-2PN. (b) Correct pixels. (c) Probability image. (d) cTTI-Method2-2PN. (e) Correct pixels. (f) Probability image. (g) cTTI-Method1-9PN. (h) Correct pixels. (i) Probability image. (j) cTTI-Method2-9PN. (k) Correct pixels. (l) Probability image.

TABLE II
VALUES OF THE ELECTROMAGNETIC PROPERTIES (REAL AND IMAGINARY PARTS OF THE RELATIVE COMPLEX PERMITTIVITY) OF THE BREAST TISSUES AT 1.1 GHZ

Tissue	ϵ_r	ϵ_i
Skin [36]	35	-23
Fat [5]	12.6	-10.13
Glandular [5]	32.7	-20.92
Tumor [5]	53.4	-18.8
Cyst [35]	60	-16.34

We consider $\pm 10\%$ variation for these values.

the variation of the imaginary part of the complex permittivity with respect to frequency of operation using the so-called Maxwell model [41].

3) *First Phantom (Phantom With a Medium-Sized Tumor):* The true TTI and the complex permittivity of this phantom are shown in Fig. 2(a) and the top row of Fig. 9. The reconstruction of the complex permittivity for the case that the data are contaminated with 9% noise is shown in the bottom row of Fig. 9. The PDF, single-property TTI, and its probability image for the real and imaginary parts of complex permittivity are shown in

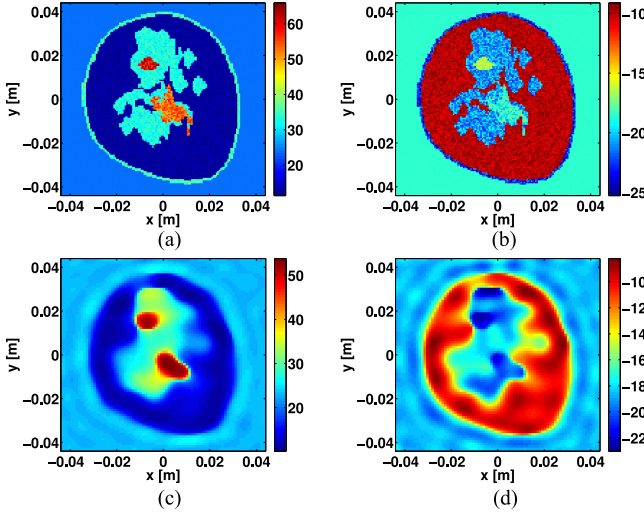


Fig. 9. First and second rows correspond to the true and reconstructed real and imaginary parts of the complex permittivity for the case that the noise is 9%. (a) True ϵ_r . (b) True ϵ_i . (c) Reconstructed ϵ_r . (d) Reconstructed ϵ_i .

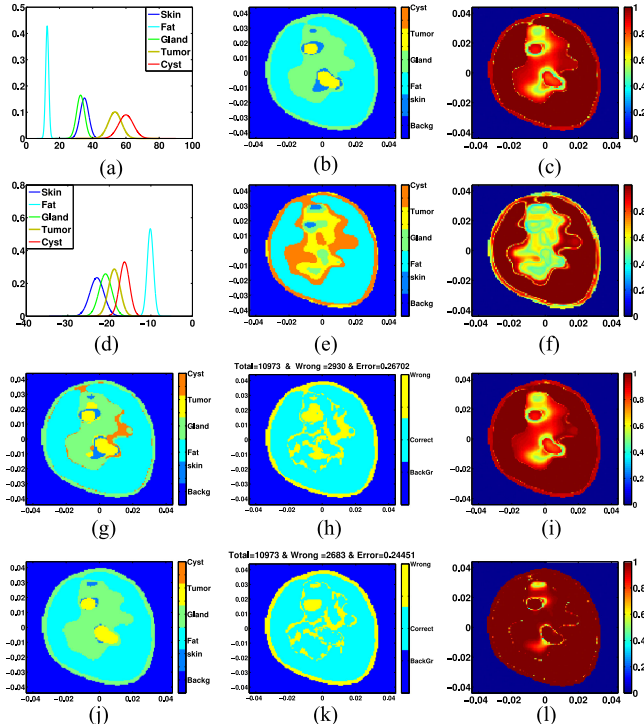


Fig. 10. First and second rows correspond to a single-property TTI for the ϵ_r and ϵ_i , respectively. The third and fourth rows correspond to the cTTI and its probability using Methods 1 and 2, respectively. (a) PDF ϵ_r . (b) Single-property TTI- ϵ_r . (c) Probability image ϵ_r . (d) PDF ϵ_i . (e) Single-property TTI- ϵ_i . (f) Probability image ϵ_i . (g) cTTI-Method 1. (h) Correct pixels. (i) Probability image. (j) cTTI-Method 2. (k) Correct pixels. (l) Probability image.

the first and second rows of Fig. 10. The cTTI using Methods 1 and 2 are shown in the third and fourth rows of Fig. 10.

4) Second Phantom (Dense Breast With Two Tumors): The true TTI and electromagnetic properties for this phantom are shown in Fig. 2(b) and the first row of Fig. 11. The recon-

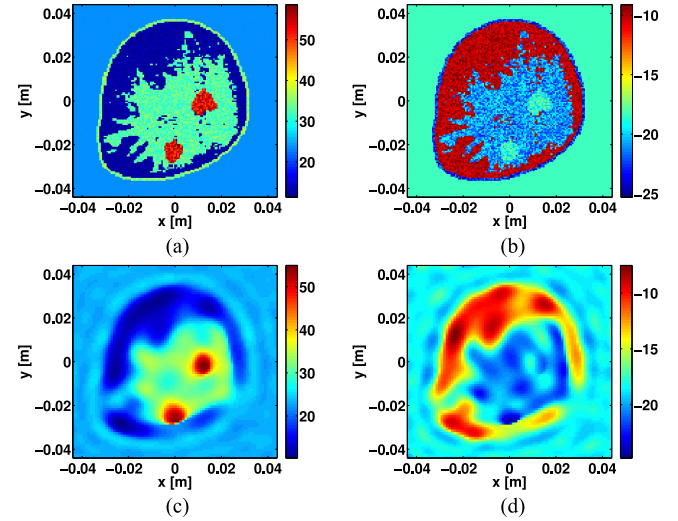


Fig. 11. First and second rows correspond to the true and reconstruction of real and imaginary parts of permittivity for the case that the noise percentage is 9%. (a) True ϵ_r . (b) True ϵ_i . (c) Reconstructed ϵ_r . (d) Reconstructed ϵ_i .

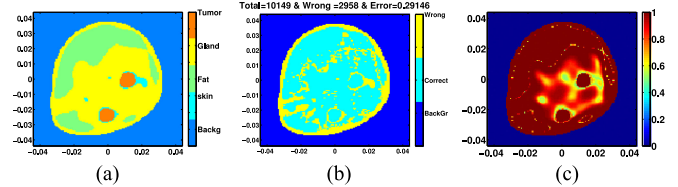


Fig. 12. cTTI, correct pixel, and probability images obtained using Method 2 for the second phantom using MWT properties. (a) cTTI-Method 2. (b) Correct pixels. (c) Probability image.

struction of the complex permittivity for the case that the data is contaminated with 9% noise is shown in the second row of Fig. 11. The cTTI, true pixel, and probability images obtained using Method 2 are shown in Fig. 12.

C. cTTI for Combined UT and MWT

We now consider the case where both UT and MWT properties are utilized together to create a composite TTI. The first phantom with a true TTI shown in Fig. 2(a) is utilized in this example. The true UT and MWT properties for this phantom are shown in the top row of Figs. 3 and 9, respectively. The data for both UT and MWT are contaminated with 9% noise. The reconstruction of the UT properties and MWT properties for 9% noise are shown in the first row of Fig. 14 and the bottom row of Fig. 9, respectively. The cTTI obtained using Method 2 for UT properties is shown in the last row of Fig. 14. The cTTI obtained using Method 2 for MWT properties is shown in the last row of Fig. 10.

Next, both UT and MWT properties are simultaneously utilized based on Method 2 to create a cTTI. The result of the cTTI using UT and MWT properties is shown in Fig. 13. As can be seen, the cTTI using both UT and MWT properties leads to a better reconstruction in comparison with the cTTIs based solely on UT properties or MWT properties. It should be noted

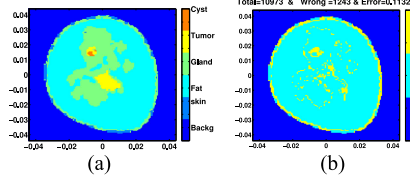


Fig. 13. Composite TTI, correct pixel, and probability images obtained using Method 2 for the case that both UT and MWT properties are utilized. (a) cTTI-Method 2. (b) Correct pixels. (c) Probability image.

that the cyst region is not detected in the cTTIs using UT and MWT separately. However, when both UT and MWT properties are simultaneously utilized, some parts of cyst region start to appear in the cTTI. Furthermore, note that the probabilities of those pixels which are mistakenly assigned as tumor (instead of cyst) are low. That is, even in the case of wrong reconstruction for some pixels, the fact that one cannot be confident in the reliability of the reconstructed tissue type for those pixels is indicated in the composite probability image.

It should be noted that the fat region is well distinguished using the single-property compressibility TTI with high probability values as shown in the second row of Fig. 14. Therefore, for the previous example, we utilized this information to provide better prior probabilities for those pixels. To this end, we gave higher prior probabilities for fat compared to other tissues for those pixels.

D. Enhanced Reconstruction Using TTI

Next, we show that the concept of TTI can be used to enhance the quantitative reconstruction. As will be explained below, in this approach, we use the TTI to create a better initial guess for the inversion algorithm. That is, the TTI concept is used as a feedback mechanism: we first reconstruct the quantitative properties using a blind initial guess (e.g., an initial guess of zero which was used in all the examples above), form the TTI images, and then, finally, use these TTI images to create a better initial guess for the inversion algorithm so as to converge to a more accurate quantitative reconstruction. It should be noted that the choice of initial guess is important for the success of inversion algorithms as a bad choice for the initial guess may cause the inversion algorithm to be trapped in wrong local minima.

The proposed method to create a good initial guess for each property can be explained as follows. For a given property, say compressibility, consider its corresponding single-property TTI and its associated probability image. Now, consider one pixel of this single-property compressibility TTI. If its corresponding probability value is above a threshold level, say 0.9, we consider this as a “fit” pixel. Therefore, for that pixel, we use its corresponding reconstructed compressibility value in our initial guess. Otherwise, for that pixel, we consider the single-property TTI of the next property, say attenuation. For that pixel, if the corresponding attenuation probability value is greater than the threshold level, we consider the tissue-type of that pixel as a “fit” tissue type and assign this pixel a compressibility value as the average of the expected minimum and maximum com-

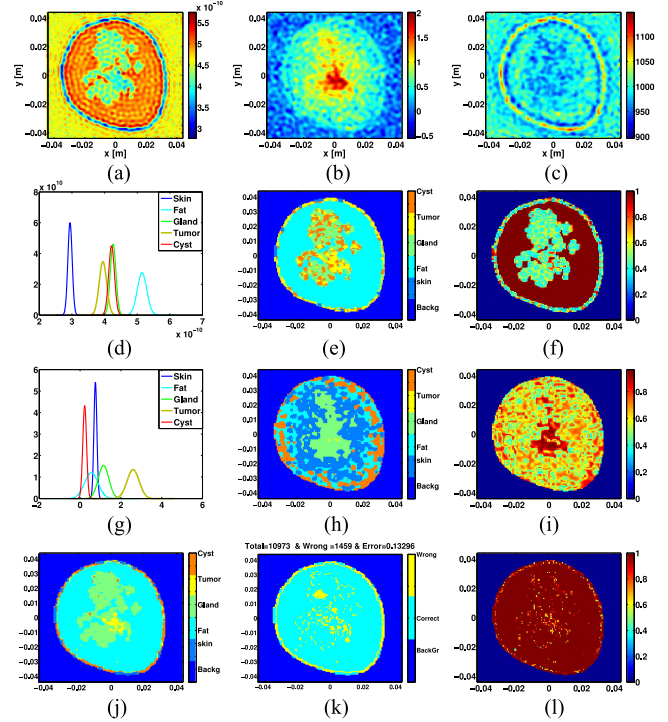


Fig. 14. First row corresponds to the reconstruction of ultrasonic properties for the case that the noise level is 9%. The second and third rows correspond to the PDF, single-property TTI, and probability image for κ and α , respectively. The last row corresponds to the composite TTI, correct pixel, and probability images obtained from Method 2. (a) Reconstructed κ . (b) Reconstructed α . (c) Reconstructed ρ . (d) PDF κ . (e) Single-property TTI- κ . (f) Probability image κ . (g) PDF α . (h) Single-property TTI- α . (i) Probability image α . (j) cTTI-Method 2. (k) Correct pixels. (l) Probability image.

pressibility values of that tissue. This process continues until we cover all the single-property TTIs. If the probability value of that pixel is never above the threshold level, we simply use the reconstructed values as there is no “smart” estimate on the value of that pixel. This procedure continues until all the properties associated with each pixel are estimated. Then, the resulting initial guess will be provided to the inversion algorithm.

To understand this approach better, we apply it to the first MRI-based phantom in the UT framework. For this case, we consider that the UT data are contaminated with 9% noise. The reconstruction of the UT properties is shown in the first row of Fig. 14. (These have been obtained assuming a zero initial guess.) The PDF, tissue type, and probability images for compressibility and attenuation property using Method 1 based on each single property are shown in the second and third rows of Fig. 14. The composite image, correct-pixel image, as well as probability image using the κ and α based on Method 2 are shown in Fig. 14. We then apply our method to create an enhanced initial guess. To this end, we utilize the single-property TTI and probability images obtained from κ and α . We also utilize the composite TTI obtained from κ and α using Method 2 to create an initial guess for the density property. The initial guess obtained from this method for compressibility, attenuation and density are shown in the first row of Fig. 15. The reconstruction of the US properties using this initial guess

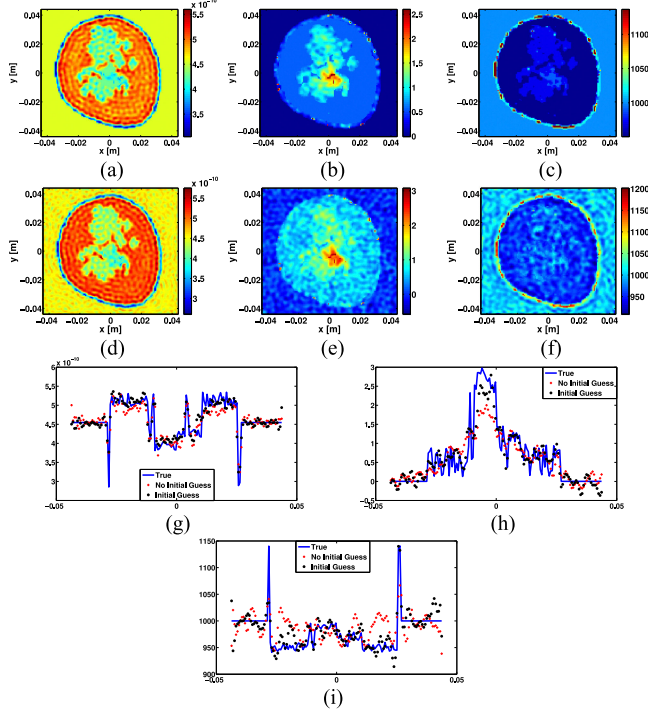


Fig. 15. First row corresponds to the initial guess provided by TTI. The second row corresponds to the reconstruction of the properties using this initial guess. The third and fourth rows correspond to the diagonal cut for the true and the reconstruction with and without using an initial guess. (a) Initial Guess- κ . (b) Initial Guess- α . (c) Initial Guess- ρ . (d) Reconstructed κ . (e) Reconstructed α . (f) Reconstructed ρ . (g) Diagonal cut κ . (h) Diagonal cut α . (i) Diagonal cut ρ .

is shown in the second row of Fig. 15. The diagonal cut from top left to the bottom right for the true previous reconstruction and the reconstruction using the initial guess provided by TTI are shown in the third and fourth rows of Fig. 15. Comparing this result with the previous reconstruction shown in the first row of Fig. 14, it can be seen that all the property reconstructions are improved. For example, the density reconstruction is significantly improved, the attenuation is also improved, and the value of the tumor attenuation is now more accurate.

V. CONCLUSION

We have introduced the concept of composite TTI and probability image for UT, MWT, and their combination. To arrive at the composite TTI, we have utilized reconstructed quantitative images, and the PDFs associated with these properties for different tissue types. The reconstructed quantitative properties are obtained by the use of inverse scattering algorithms, whereas the PDFs are constructed based on the expected range of values that tissue properties can take. Specifically, we have utilized two methods to create the composite TTI. The first method utilizes the single-variate PDF of each tissue property whereas the second method uses the multivariate PDF for the all tissue properties. For the examples considered here, Method 2 outperformed Method 1 in creating the composite TTI. The main advantage of the proposed concept is that it integrates

all the quantitative information of the reconstructed property images into one composite image that represents the most probable tissue type at each pixel. The use of multimodality imaging based on multiphysics properties provides and enhanced ability to identify tissue types within images and better reveals their structure. This will have important advantages for the diagnosis of disease by physicians.

REFERENCES

- [1] P. Huthwaite and F. Simonetti, "High-resolution imaging without iteration: A fast and robust method for breast ultrasound tomography," *J. Acoust. Soc. Amer.*, vol. 130, no. 3, pp. 1721–1734, 2011. [Online]. Available: <http://scitation.aip.org/content/asa/journal/jasa/130/3/10.1121/1.3613936>
- [2] C. Li, N. Duric, and L. Huang, "Comparison of ultrasound attenuation tomography methods for breast imaging," *Proc. SPIE*, vol. 6920, pp. 692015-1–692015-9, 2008.
- [3] C. Li, N. Duric, P. Littrup, and L. Huang, "In vivo breast sound-speed imaging with ultrasound tomography," *Ultrasound Med. Biol.*, vol. 35, no. 10, pp. 1615–1628, 2009.
- [4] P. Mojabi and J. LoVetri, "Enhancement of the Krylov subspace regularization for microwave biomedical imaging," *IEEE Trans. Med. Imag.*, vol. 28, no. 12, pp. 2015–2019, Dec. 2009.
- [5] T. Rubk, P. Meaney, P. Meincke, and K. Paulsen, "Nonlinear microwave imaging for breast-cancer screening using gauss newton's method and the CGLS inversion algorithm," *IEEE Trans. Antennas Propag.*, vol. 55, no. 8, pp. 2320–2331, Aug. 2007.
- [6] Z. Q. Zhang and Q. H. Liu, "Three-dimensional nonlinear image reconstruction for microwave biomedical imaging," *IEEE Trans. Biomed. Eng.*, vol. 51, no. 3, pp. 544–548, Mar. 2004.
- [7] Z. Q. Zhang, Q. H. Liu, C. Xiao, E. Ward, G. Ybarra, and W. Joines, "Microwave breast imaging: 3-D forward scattering simulation," *IEEE Trans. Biomed. Eng.*, vol. 50, no. 10, pp. 1180–1189, Oct. 2003.
- [8] T. Grzegorczyk, P. Meaney, P. Kaufman, R. di Florio-Alexander, and K. Paulsen, "Fast 3-D tomographic microwave imaging for breast cancer detection," *IEEE Trans. Med. Imag.*, vol. 31, no. 8, pp. 1584–1592, Aug. 2012.
- [9] Y. M. Wang and W. C. Chew, "An iterative solution of the two-dimensional electromagnetic inverse scattering problem," *Int. J. Imag. Syst. Technol.*, vol. 1, no. 1, pp. 100–108, 1989. [Online]. Available: <http://dx.doi.org/10.1002/ima.1850010111>
- [10] P. Mojabi and J. LoVetri, "Ultrasound tomography for simultaneous reconstruction of acoustic density, attenuation, and compressibility profiles," *J. Acoust. Soc. Amer.*, vol. 137, no. 4, pp. 1813–1825, 2015.
- [11] M. Moghaddam and W. C. Chew, "Simultaneous inversion of compressibility and density in the acoustic inverse problem," *Inverse Problems*, vol. 9, no. 6, pp. 715–730, 1993.
- [12] M. Haynes and M. Moghaddam, "Large-domain, low-contrast acoustic inverse scattering for ultrasound breast imaging," *IEEE Trans. Biomed. Eng.*, vol. 57, no. 11, pp. 2712–2722, Nov. 2010.
- [13] W. Chew and Y. Wang, "Reconstruction of two-dimensional permittivity distribution using the distorted Born iterative method," *IEEE Trans. Med. Imag.*, vol. 9, no. 2, pp. 218–225, Jun. 1990.
- [14] R. J. Lavarello and M. L. Oelze, "Density imaging using inverse scattering," *J. Acoust. Soc. Am.*, vol. 125, no. 2, pp. 793–802, Feb. 2009.
- [15] R. Lavarello and M. Oelze, "A study on the reconstruction of moderate contrast targets using the distorted Born iterative method," *IEEE Trans. Ultrason., Ferroelectr. Freq. Control*, vol. 55, no. 1, pp. 112–124, Jan. 2008.
- [16] A. J. Hesford and W. C. Chew, "Fast inverse scattering solutions using the distorted Born iterative method and the multilevel fast multipole algorithm," *J. Acoust. Soc. Amer.*, vol. 128, no. 2, pp. 679–690, Jun. 2010.
- [17] P. M. van den Berg and R. E. Kleinman, "A contrast source inversion method," *Inverse Problems*, vol. 13, no. 6, p. 1607, 1997. [Online]. Available: <http://stacks.iop.org/0266-5611/13/i=6/a=013>
- [18] K. W. A. van Dongen and W. M. D. Wright, "A full vectorial contrast source inversion scheme for three-dimensional acoustic imaging of both compressibility and density profiles," *J. Acoust. Soc. Amer.*, vol. 121, no. 3, pp. 1538–1549, 2007. [Online]. Available: <http://scitation.aip.org/content/asa/journal/jasa/121/3/10.1121/1.2431333>

- [19] A. Tikhonov and V. Arsenin, *Solutions of Ill-Posed Problems* (ser. Scripta Series in Mathematics). Great Falls, MT, USA: Winston, 1977.
- [20] T. Tran-Duc, N. Linh-Trung, and M. Do, "Modified distorted Born iterative method for ultrasound tomography by random sampling," in *Proc. Int. Symp. Commun. Inf. Technol.*, Oct. 2012, pp. 1065–1068.
- [21] T. Tran-Duc, N. Linh-Trung, M. L. Oelze, and M. N. Do, "Application of L_1 regularization for high-quality reconstruction of ultrasound tomography," *Proc. 4th Int. Conf. Biomed. Eng. Vietnam*, 2013, pp. 309–312.
- [22] S. J. Kim, K. Koh, M. Lustig, S. Boyd, and D. Gorinevsky, "An Interior-point method for large-scale l_1 -regularized least squares," *IEEE J. Sel. Topics Signal Process.*, vol. 1, no. 4, pp. 606–617, Dec. 2007.
- [23] A. Abubakar, P. van den Berg, T. Habashy, and H. Braunisch, "A multiplicative regularization approach for deblurring problems," *IEEE Trans. Image Process.*, vol. 13, no. 11, pp. 1524–1532, Nov. 2004.
- [24] P. M. van den Berg, A. Abubakar, and J. T. Fokkema, "Multiplicative regularization for contrast profile inversion," *Radio Sci.*, vol. 38, no. 2, p. 8022, 2003.
- [25] P. C. Hansen, *Rank-Deficient and Discrete Ill-Posed Problems: Numerical Aspects of Linear Inversion*. Philadelphia, PA, USA: SIAM, 1998.
- [26] P. Hansen, "The truncated SVD as a method for regularization," *BIT Numerical Math.*, vol. 27, no. 4, pp. 534–553, 1987.
- [27] P. Mojabi, "Ultrasound tomography: An inverse scattering approach," M.Sc. thesis, Univ. Manitoba, Winnipeg, MB, Canada, 2014.
- [28] P. Mojabi and J. LoVetri, "Microwave and ultrasound imaging for biomedical tissue identification," in *Proc. USNC-URSI Radio Sci. Meeting (Joint AP-S Symp.)*, Jul. 2014, pp. 56–56.
- [29] P. Mojabi and J. LoVetri, "Tissue-type imaging using ultrasound tomography," in *Proc. IEEE MTT-S Int. Conf. Numerical Electromagn. Multiphys. Model. Optim.*, Aug. 2015, pp. 1–3.
- [30] M. Andr, C. Barker, N. Sekhon, J. Wiskin, D. Borup, and K. Callahan, "Pre-clinical experience with full-wave inverse-scattering for breast imaging," in *Acoustical Imaging* (ser. Acoustical Imaging), vol. 29, I. Akiyama, Ed. Dordrecht, Netherlands: Springer, 2009, pp. 73–80. [Online]. Available: http://dx.doi.org/10.1007/978-1-4020-8823-0_10
- [31] J. Mamou and M. L. Oelze, *Quantitative Ultrasound in Soft Tissues*. New York, NY, USA: Springer, 2013.
- [32] E. L. Madsen, M. A. Hobson, G. R. Frank, H. Shi, J. Jiang, T. J. Hall, T. Varghese, M. M. Doyley, and J. B. Weaver, "Anthropomorphic breast phantoms for testing elastography systems," *Ultrasound Med. Biol.*, vol. 32, no. 6, pp. 857–874, 2006.
- [33] E. L. Madsen, J. A. Zagzebski, and G. R. Frank, "An anthropomorphic ultrasound breast phantom containing intermediate sized scatterers," *Ultrasound Med. Biol.*, vol. 8, no. 4, pp. 381–392, 1982.
- [34] H. Azhari, *Basics of Biomedical Ultrasound for Engineers*. Hoboken, NJ, USA: Wiley, 2010. [Online]. Available: <http://books.google.ca/books?id=FeauV7dDCoC>
- [35] M. Lazebnik, D. Popovic, L. McCartney, C. B. Watkins, M. J. Lindstrom, J. Harter, S. Sewall, T. Ogilvie, A. Magliocco, T. M. Breslin, W. Temple, D. Mew, J. H. Booske, M. Okoniewski, and S. C. Hagness, "A large-scale study of the ultrawideband microwave dielectric properties of normal, benign and malignant breast tissues obtained from cancer surgeries," *Phys. Med. Biol.*, vol. 52, no. 20, pp. 6093–6115, 2007.
- [36] S. Hagness, A. Taflowe, and J. E. Bridges, "Two-Dimensional FDTD analysis of a pulsed microwave confocal system for breast cancer detection: Fixed-focus and antenna-array sensors," *IEEE Trans. Biomed. Eng.*, vol. 45, no. 12, pp. 1470–1479, Dec. 1998.
- [37] P. Mojabi and J. LoVetri, "Microwave biomedical imaging using the multiplicative regularized Gauss–Newton inversion," *IEEE Antennas Wireless Propag. Lett.*, vol. 8, pp. 645–648, 2009.
- [38] R. O. Duda, P. E. Hart, and D. G. Stork, *Pattern Classification*, 2nd ed. New York, NY, USA: Wiley-Interscience, 2000.
- [39] D. Kurrant and E. Fear, "Regional estimation of the dielectric properties of inhomogeneous objects using near-field reflection data," *Inverse Problems*, vol. 28, no. 7, 2012, Art. no. 075001. [Online]. Available: <http://stacks.iop.org/0266-5611/28/i=7/a=075001>
- [40] A. Abubakar, P. Van den Berg, and S. Semenov, "A robust iterative method for born inversion," *IEEE Trans. Geosci. Remote Sens.*, vol. 42, no. 2, pp. 342–354, Feb. 2004.
- [41] A. Abubakar, P. M. van den Berg, and T. M. Habashy, "Application of the multiplicative regularized contrast source inversion method on TM- and TE-polarized experimental Fresnel data," *Inverse Problems*, vol. 21, no. 6, p. S5, 2005. [Online]. Available: <http://stacks.iop.org/0266-5611/21/i=6/a=S02>



Pedram Mojabi (M'14–GSM'15) received the M.Sc. degree in electrical engineering from the University of Manitoba, Winnipeg, MB, Canada, in 2014, where he is currently working toward the Ph.D. degree in electrical engineering.

His current research interests are computational ultrasonics, computational electromagnetics, ultrasound tomography, microwave tomography, and multiphysics imaging.

Mr. Mojabi is an Engineer in Training at the Engineers Geoscientists Manitoba. From 2012 to 2014, he served as the Vice Chair of the IEEE Winnipeg Waves chapter.



Joe LoVetri (S'84–M'84–SM'09) received the Ph.D. degree from the University of Ottawa, Ottawa, ON, Canada, in 1991.

From 1984 to 1986, he was an EMI/EMC Engineer at Sperry Defence Division, Winnipeg, MB, Canada, and from 1986 to 1988, he was a TEMPEST Engineer at the Communications Security Establishment, Ottawa, Canada. From 1988 to 1991, he was a Research Officer at the Institute for Information Technology, National Research Council of Canada. From 1991 to 1999, he was with the Department of Electrical and

Computer Engineering, The University of Western Ontario. In 1997/1998, he spent a sabbatical year at the TNO Physics and Electronics Laboratory, Netherlands. In 1999, he joined the University of Manitoba, Winnipeg, where he is currently a Professor and Head of the Department of Electrical and Computer Engineering. From 2004 to 2009, he was the Associate Dean (Research and Graduate Programs) for the Faculty of Engineering. His main research interests include computational electromagnetics, inverse problems, microwave and ultrasound imaging, and biomedical imaging.

Dr. LoVetri received an URSI Young Scientist Award in 1993, the 2000 IEEE EMC Best Symposium Paper Award, and the 2007 ACES Outstanding Paper Award. In 2002, he received the University of Manitoba Rh Award for Outstanding Contributions to Scholarship and Research in the Applied Sciences. From 2005 to 2009, he was the National Representative for Commission E on the Canadian National Committee of URSI. He is the Chapter Chair for the IEEE EMC Ottawa Chapter as well as the Winnipeg Waves Chapter (AP/MTT). He has been a Registered Professional Engineer in Canada since 1994.